

Generation of heralded entanglement between distant hole spins

Aymeric Delteil^{1*}, Zhe Sun^{1*}, Wei-bo Gao^{1,2*}, Emre Togan¹, Stefan Faelt¹, and Ataç Imamoglu^{1†}

¹*Institute of Quantum Electronics, ETH Zurich, 8093 Zurich, Switzerland*

²*Div. of Physics and Applied Physics, Nanyang Tech. Univ., Singapore 637371*

**These authors contributed equally to this work.*

†Corresponding author. E-mail: imamoglu@phys.ethz.ch

Quantum entanglement emerges naturally in interacting quantum systems and plays a central role in quantum information processing [1–4]. Remarkably, it is possible to generate entanglement even in the absence of direct interactions: provided that which path information is erased, weak spin-state dependent light scattering can be used to project two distant spins onto a maximally entangled state upon detection of a single photon [5]. Even though this approach is necessarily probabilistic, successful generation of entanglement is heralded by the photon detection event. Here, we demonstrate heralded quantum entanglement [6–9] of two quantum dot heavy-hole spins separated by 5 meters using single-photon interference. Thanks to the long coherence time of hole spins and the efficient spin-photon interface provided by self-assembled quantum dots [10–12] embedded in leaky microcavity structures, we generate 2300 entangled spin pairs per second, which represents an improvement approaching three orders of magnitude as compared to prior experiments [13]. Delayed two-photon interference scheme we developed allows for efficient verification of quantum correlations. Our results lay the groundwork for the realization of quantum networks in semiconductor nanostructures. Combined with schemes for transferring quantum information to a long-lived memory qubit [14], fast entanglement generation we demonstrate could also impact quantum repeater architectures.

In contrast to prior experiments demonstrating electron spin photon entanglement [10–12], our experiments are based on heavy-hole pseudo-spins in self-assembled quantum dots (QD) that have been shown to exhibit long coherence times [15–18]. Figure 1a depicts our experimental set-up incorporating two QDs separated by 5 meters that are resonantly driven by weak 3.2 ns long pulses from a Ti:Sapphire laser, termed the entanglement laser. Additional diode laser pulses ensure

that each QD is optically charged with a single excess heavy-hole and that the hole pseudo-spin is prepared in the requisite state. The QDs are embedded in distributed Bragg reflector (DBR) structures [19] that allow for efficient collection of the generated resonance fluorescence.

Figure 1b shows the relevant energy-level diagram as well as the allowed optical transitions for single-hole charged QDs when an external magnetic field (B_x) is applied perpendicular to the growth direction (Voigt geometry) [20, 21]. The initial states of the optical transitions in the single-hole charged regime are metastable states identified by the orientation of the hole pseudo-spin, with $|\uparrow\rangle$ ($|\downarrow\rangle$) denoting hole angular momentum projection. Presence of $B_x \neq 0$ yields a finite splitting of the pseudo-spin states due to heavy-light hole mixing [22]. Spontaneous emission of a V (H) polarized photon at frequency ω_{blue} (ω_{diag1}) from the trion state $|T_b\rangle$ at rate $\Gamma/2$ brings the QD back into the $|\downarrow\rangle$ ($|\uparrow\rangle$) state. Due to these selection rules, addressing any of the four allowed transitions with a single laser will efficiently transfer the spin population into the opposite ground state within a few optical cycles. Since the intensity of entanglement laser is chosen to be well below saturation, the ensuing optical transitions lead to either V-polarized Rayleigh scattering or H-polarized Raman scattering.

The light propagation time from the first beam splitter (BS1) to both dots, as well as from the dots to the second beam splitter (BS2) are rendered nearly identical, such that the photons scattered by the two dots during a single entanglement laser pulse recombine at the same time on the second beam splitter. When both QDs are initially prepared in the $|\downarrow\rangle$ state, the simultaneous weak excitation of the blue transitions will lead to either a spontaneous Raman or Rayleigh scattering event with a probability $\varepsilon^2 \ll 1$, leaving the system in the state

$$|\Psi\rangle_{12} = \frac{1}{\sqrt{2}}[|\downarrow, 0\rangle + \varepsilon e^{-i\theta_1}(|\uparrow, 1_H\rangle + |\downarrow, 1_V\rangle)]_{QD1} \otimes [|\downarrow, 0\rangle + \varepsilon e^{-i\theta_2}(|\uparrow, 1_H\rangle + |\downarrow, 1_V\rangle)]_{QD2}. \quad (1)$$

To ensure that a click in one of the single-photon detectors stem from detection of a H-polarized Raman scattered photon at frequency ω_{diag1} , we placed transmission gratings and Fabry-Pérot filters in front of the detectors (Fig. 1a). In this case, detection of a single (Raman) photon projects the composite system wave-function onto the maximally entangled state

$$|\Psi\rangle_{12} = \frac{1}{\sqrt{2}}[|\uparrow, \downarrow\rangle + e^{-i\theta}|\downarrow, \uparrow\rangle] \quad (2)$$

in the limit where two photon scattering probability ε^4 is vanishingly small. Provided that the Zeeman splitting in the two QDs are rendered identical, the relative phase $\theta = \theta_2 - \theta_1$ is time-

independent and is primarily determined by the optical path length difference between the two arms from BS1 to BS2 (Fig. 1a).

The entanglement generation scheme we use relies crucially on the indistinguishability of the photons emitted by two remote QDs such that "which-path" information is not available in the single-photon interferometer depicted in Fig. 1a. After locating a pair of QDs (QD1 and QD2) with similar transition energies, we ensure that the optical transition frequencies ω_{blue} and ω_{diag1} are identical for QD1 and QD2; this is achieved by tuning both electric and magnetic fields applied on the two QDs separately. The indistinguishability of the Raman scattered photons is characterized by a Hong-Ou-Mandel (HOM) experiment [23] under pulsed excitation of the blue transition where we monitor the coincidence events at the two single photon detectors. Figure 1c shows that two-photon interference results in a strong decrease of the two-fold coincidence rate associated with the central peak when the two input photons have parallel polarizations. The associated interference visibility deduced from this measurement is $91 \pm 6 \%$.

For the protocol we implement, it is essential that the QD spins remain coherent during the time it takes for the heralding process to be completed. In our scheme this time is determined predominantly by the 21.7 ns propagation time from the QDs to the single-photon detectors. To demonstrate that the hole pseudo-spin retains its coherence on this timescale, we implemented a quantum optical measurement technique. It is well known in quantum optics that while first-order coherence properties of Rayleigh scattering follows that of the excitation laser [24, 25], the coherence of spin-flip Raman scattering is determined both by the laser and the spin coherence [26]. The latter is a consequence of the fact that the quantum field $E^{(+)}(t)$ generated in Raman scattering is linearly proportional to the spin raising operator $\sigma_{\uparrow\downarrow}(t - R/c)$, where R denotes the distance between the QD and the detector. Therefore, hole spin coherence (T_2^*) time can be determined by measuring the coherence time of Raman scattered photons, provided that the excitation laser has a much longer coherence time.

To perform this experiment, we use the set-up depicted in Fig. 2a, where the emitted photons at a desired wavelength are filtered and then sent into a stabilized Mach-Zehnder interferometer whose path length difference is set to 22 ns. We apply the pulse sequence depicted in Fig. 2b: the spin is first prepared in the $|\downarrow\rangle$ state by spin pumping using the red (vertical) transition. We then apply two weak pulses on the blue transition, separated by the same time as the path length difference, such that the light scattering amplitudes during the two pulses can interfere at the second beam

splitter. The detector is then gated so that it measures only in this interference time window and the photon detection events are recorded as a function of the phase difference between the two arms. As a reference, we measure an interference visibility of 83 % for the excitation laser, limited by the precision with which we stabilize the optical path length difference. For Raman photons we obtain an interference visibility of 38.9 % for QD1 and 29.5 % for QD2, which is more than half the visibility measured for Rayleigh scattering (66.7 % for QD1 and 54.8 % for QD2). The visibility of Rayleigh photons is limited by a contribution from incoherent light scattering, whereas Raman coherence is in addition reduced by the decay of spin coherence. This result demonstrates that both spins retain a sizeable degree of coherence during a time-window of 22 ns and that the reduced visibility is mainly due to the contribution from incoherent light scattering.

The fringes in the aforementioned Mach-Zehnder interferometer could also be observed by varying the phase of the hole pseudo-spin. The latter can be adjusted using a V-polarized off-resonant laser field that induces different phases on the two spin states due to different magnitude of the ac-Stark effect. We carried out this experiment on QD1 by applying a laser that is red-detuned by ~ 20 GHz from the red and ~ 50 GHz from the blue vertical transition (bottom right diagram of Fig. 2d). The difference in the ac-Stark shift experienced by the two transitions allows the state $|\downarrow\rangle$ to accumulate a phase $\varphi = \Omega^2\tau\delta/4\Delta(\Delta + \delta)$, relative to $|\uparrow\rangle$. Here, Ω is the Rabi frequency of the laser, τ the pulse duration, Δ the detuning from the red transition and $\delta = \omega_{blue} - \omega_{red}$ the energy difference between the two transitions. In order to characterize the effect of spin-phase rotation, we repeat the interferometric measurement while keeping the optical path-length difference constant and applying a 4 ns-long detuned laser pulse in between the two weak excitation pulses (Fig. 2d). By varying the laser power from 0 to $\sim 2 \mu\text{W}$, we change the relative phase of the two spin states and thus the relative phase of the Raman scattering amplitude before and after the pulse that induces the spin-state dependent ac-Stark shift. The oscillations in the count rate as a function of the laser power (Fig. 2e, black dots) unequivocally demonstrate single pseudo-spin rotation about the z axis of the Bloch sphere. The red curve in Fig. 2e is a sinusoidal fit to the data, showing that no sizable loss of visibility is observed for spin rotation up to 4π .

Having demonstrated that hole spin coherence persists for longer than 22 ns, we address the verification of heralded spin-spin entanglement. To demonstrate classical correlations between the distant spins, we carry out local single-spin measurement in the computational basis, conditioned upon the detection of a Raman photon during the entanglement pulse. We benefit from the fact

that each spin state can be excited to a corresponding trion state with the same oscillator strength and the same laser polarization but using a different resonant laser wavelength. The detection of a photon during a blue (red) laser pulse thus tells with a high confidence level that the state of the spin prior to the measurement pulse was $|\downarrow\rangle$ ($|\uparrow\rangle$). In order to measure the four different spin combinations under the same experimental conditions, we alternate in a single experiment four pulses sequences, each performing one of the four requisite measurement combinations. The full pulse sequence is described in Fig. 3a: we first prepare the state $|\downarrow, \downarrow\rangle$ by spin pumping, then apply the weak entanglement laser pulse. The detection of a Raman photon during this pulse heralds successful entanglement generation. We then successively measure the state of the two dots. The measurement pulses of the two dots are offset in time, allowing us to extract which-path information. All the measurements are performed close to saturation and the detection efficiencies are rendered similar. The duration of the full sequence is 4×104 ns. Figure 3b shows the results of the 3-fold coincidences detected during 106.5 hours of measurement. As expected, the odd parity events, where the spins of the two dots are opposite, are much more likely than the even parity events, where the two spins are found in the same state. The associated fidelity is $F_z = 80.6 \pm 6.6$ %.

To demonstrate quantum correlations between the two distant spins, we implement a delayed two-photon interference experiment. The key element of this approach for verifying quantum correlations is the possibility to rotate one of the spins along the z-axis after heralded spin entanglement is generated. Application of a detuned laser pulse on QD1 as described earlier, results in rotating the phase of the entangled state by $\alpha(\tau)$ so that the the entangled state becomes $(|\uparrow, \downarrow\rangle + e^{-i\theta - i\alpha(\tau)}|\downarrow, \uparrow\rangle)/\sqrt{2}$. Subsequent application of a second weak (measurement) pulse, that is identical in intensity and duration to the entanglement pulse, on both QDs simultaneously leads to

$$|\Psi\rangle_{12} = \frac{1}{\sqrt{2}}[|\uparrow, \downarrow, 0\rangle + \varepsilon e^{-i\theta_2}|\uparrow, \uparrow, 1_H\rangle + e^{-i\theta - i\alpha(\tau)}(\varepsilon e^{-i\theta_1}|\uparrow, \uparrow, 1_H\rangle + |\downarrow, \uparrow, 0\rangle)] \quad (3)$$

$$= \frac{\varepsilon}{\sqrt{2}} e^{-i\theta_2} (1 + e^{-i\alpha(\tau)}) |\uparrow, \uparrow, 1_H\rangle + \frac{1}{\sqrt{2}} \left(|\uparrow, \downarrow, 0\rangle + e^{-i\theta - i\alpha(\tau)} |\downarrow, \uparrow, 0\rangle \right). \quad (4)$$

Therefore, conditioned on an initial Raman photon detection event that heralded spin-spin entanglement, the detection of a second time-delayed Raman photon detection probability scales as $\varepsilon^2 |1 + e^{-i\alpha(\tau)}|^2$. The expectation value of Raman photon detection can be shown to be

$$\langle E^{(-)} E^{(+)} \rangle \propto 1 + 0.5(\sigma_z^1 + \sigma_z^2) - \langle \sigma_{\uparrow\uparrow}^2 \sigma_{\uparrow\downarrow}^1 + \sigma_{\downarrow\uparrow}^1 \sigma_{\downarrow\downarrow}^2 \rangle. \quad (5)$$

The peak-to-peak contrast in $\langle E^{(-)}E^{(+)} \rangle$ obtained by varying $\alpha(\tau)$ therefore gives us the magnitude of non-local quantum correlations between the two spins.

To verify the presence of quantum correlations using such a delayed two-photon interference experiment, we use the pulse sequence described in Fig. 3c. We once again prepare the spins in the $|\downarrow, \downarrow\rangle$ state by spin pumping and then apply the entanglement generation pulse. The phase of the state is then modified by the detuned laser pulse, whose duration is changed within the pulse sequence by alternating eight patterns that differ only by the duration of this particular pulse. Eight evenly distributed durations are chosen to cover more than one full revolution. Finally the measurement pulse is simultaneously sent to both dots. The two-fold coincidences measured for each value of the pulse length are normalized by the uncorrelated coincidence rate obtained by measuring two photons emitted in different periods. The figure 3d presents data obtained during 180 min of measurement. The obtained ratio exhibits clear oscillations of visibility $29.6 \pm 2.8 \%$. Combining the results depicted in Figs. 3b&3d, we deduce an overall fidelity of the generated entangled state of $F = 55.2 \pm 3.5 \%$.

The non-local measurement of quantum correlations does not allow us to determine the relative phase θ between the $|\uparrow\downarrow\rangle$ and $|\downarrow\uparrow\rangle$ contributions. In the ideal limit of z-basis measurements yielding vanishing probability for $|\uparrow\uparrow\rangle$ and $|\downarrow\downarrow\rangle$ states, the state space of the two qubits is restricted to a two-dimensional subspace which can be mapped onto a Bloch sphere with $|\uparrow\downarrow\rangle$ and $|\downarrow\uparrow\rangle$ as the north and the south poles. A perfect visibility in non-local two-photon interference in return ensures that the two-spin state lives on the equator of this Bloch sphere: $|\Psi\rangle_{12} = (|\downarrow, \uparrow\rangle + e^{-i\theta}|\uparrow, \downarrow\rangle)/\sqrt{2}$. To fix the value of θ , we need to use a strong laser to stabilize the optical path length difference to an integer multiple of its wavelength immediately prior to the generation of the entangled spin state. We have implemented such a stabilization scheme to perform the Mach-Zehnder interferometry measurements depicted in Fig. 2. We emphasize that it is straightforward to extend our heralded entanglement generation experiments by fixing θ with an accuracy of $\pm\pi/10$ using this stabilization scheme while achieving nearly the same entanglement generation rate.

Our work establishes QD heavy-hole spin states as ideal candidates for quantum information processing tasks requiring a spin-photon interface: combination of long T_2^* coherence times and high photon collection efficiency yielding up to 10 million photons per second on saturated exciton transitions, yields an unprecedented spin-spin entanglement generation rate of 2300 ebits per second. This rate could be further increased by a factor of 10 using cavity QED [19]. Increasing the

distance between the entangled spin pairs could be achieved either by using dynamical decoupling or by using singlet-triplet qubits of QD molecules that exhibit longer spin coherence times while simultaneously allowing for efficient spin measurement [27]. Our results provide major motivation for investigating possibilities for coherent transfer of the hole spin to a local qubit that exhibits a longer coherence time [14] but lacks an efficient interface to propagating optical photons [28]. A hybrid system that uses QD spins for fast entanglement generation and long-lived qubits for storage could have a major impact on implementation of quantum repeaters [3]. In addition, heralded spin entanglement could provide a quantum coherent link between nodes of an on-chip quantum information processor [29, 30].

-
- [1] Nielsen, M. A. & Chuang, I. L., Quantum computation and quantum information (Cambridge Univ. Press, Cambridge, UK, 2000).
 - [2] Briegel, H.-J., Dür, W., Cirac, J. I. & Zoller, P. Quantum repeaters: the role of imperfect local operations in quantum communication. *Phys. Rev. Lett.* **81**, 5932-5935 (1998).
 - [3] Childress, L., Taylor, J. M., Sørensen, A. S. & Lukin, M. D. Fault-tolerant quantum communication based on solid-state photon emitters. *Phys. Rev. Lett.* **96**, 070504 (2006).
 - [4] Kimble, H. J. The quantum internet. *Nature* **453**, 1023-1030 (2008).
 - [5] Cabrillo, C., Cirac, J. I., García-Fernández, P. & Zoller, P. Creation of entangled states of distant atoms by interference. *Phys. Rev. A* **59**, 1025-1033 (1999).
 - [6] Moehring, D. L. *et al.* Entanglement of single-atom quantum bits at a distance. *Nature* **449**, 68-71 (2007).
 - [7] Hofmann, J. *et al.* Heralded entanglement between widely separated atoms. *Science* **337**, 72-75 (2012).
 - [8] Slodicka, L. *et al.* Atom-atom entanglement by single-photon detection. *Phys. Rev. Lett.* **110**, 083603 (2013).
 - [9] Bernien, H. *et al.* Heralded entanglement between solid-state qubits separated by three metres. *Nature* **497**, 86-90 (2013).
 - [10] Gao, W. B., Fallahi, P., Togan, E., Miguel-Sanchez, J. & Imamoglu, A. Observation of entanglement between a quantum dot spin and a single photon. *et al. Nature* **491**, 426-430 (2012).
 - [11] De Greve, K. *et al.* Quantum-dot spin-photon entanglement via frequency downconversion to telecom wavelength. *Nature* **491**, 421-425 (2012).
 - [12] Shaibley, J. R. *et al.* Demonstration of quantum entanglement between a single electron spin confined

- to an InAs quantum dot and a photon. *Phys. Rev. Lett.* **110**, 167401 (2013).
- [13] Hucul, D. *et al.* Modular entanglement of atomic qubits using photons and phonons. *Nature Phys.* **11**, 37-42 (2015).
- [14] Meyer, H.M. *et al.* Direct photonic coupling of a semiconductor quantum dot and a trapped ion. *Phys. Rev. Lett.* **114**, 123001 (2015).
- [15] Brunner, D. *et al.* A coherent single-hole spin in a semiconductor. *Science* **325**, 70-72 (2009).
- [16] De Greve, K. *et al.* Ultrafast coherent control and suppressed nuclear feedback of a single quantum dot hole qubit. *Nature Phys.* **7**, 872-878 (2011)
- [17] Greilich, K., Carter, S. G., Kim, D., Bracker, A. S. & Gammon, D. Optical control of one and two hole spins in interacting quantum dots. *Nature Photon.* **5**, 702-708 (2011).
- [18] Carter, S. G. *et al.* Strong hyperfine-induced modulation of an optically driven hole spin in an InAs quantum dot. *Phys. Rev. B* **89**, 075316 (2014).
- [19] Gazzano, O. *et al.* Bright solid-state sources of indistinguishable single photons. *Nature Comm.* **4**, 1425 (2013).
- [20] Xu, X. *et al.* Fast spin state initialization in a singly charged InAs-GaAs quantum dot by optical cooling. *Phys. Rev. Lett.* **99**, 097401 (2007).
- [21] Atatüre, M. *et al.* Quantum-dot spin-state preparation with near-unity fidelity. *Science* **312**, 551-553 (2006).
- [22] Bayer, M. *et al.* Fine structure of neutral and charged excitons in self-assembled In(Ga)As/(Al)GaAs quantum dots. *Phys. Rev. B* **65**, 195315 (2002).
- [23] Hong, C. K., Ou, Z. Y. & Mandel, L. Measurement of subpicosecond time intervals between two photons by interference. *Phys. Rev. Lett.* **59**, 2044-2046 (1987).
- [24] Loudon, R. *The quantum theory of light*, Oxford University Press, Oxford (2000).
- [25] Matthiesen, C., Vamivakas, A. N. & Atatüre, M. Subnatural linewidth single photons from a quantum dot. *Phys. Rev. Lett.* **108**, 093602 (2012).
- [26] Fernandez, G., Volz, T., Desbuquois, R., Badolato, A. & Imamoglu, A. Optically tunable spontaneous Raman fluorescence from a single self-assembled InGaAs quantum dot. *Phys. Rev. Lett.* **103**, 087406 (2009).
- [27] Weiss, K. M., Elzerman, J. M., Delley, Y. L., Miguel-Sanchez, J. & Imamoglu, A. Coherent two-electron spin qubits in an optically active pair of coupled InGaAs quantum dots. *Phys. Rev. Lett.* **109**, 107401 (2012).
- [28] Robledo, L. *et al.* High-fidelity projective read-out of a solid-state spin quantum register. *Nature* **477**, 574-578 (2011).
- [29] Reithmaier, G. *et al.* On-chip time resolved detection of quantum dot emission using integrated superconducting single photon detectors. *Science Report* **3**, 1901 (2013).

- [30] Arcari, M. *et al.* Near-unity coupling efficiency of a quantum emitter to a photonic crystal waveguide. *Phys. Rev. Lett.* **113**, 093603 (2014).

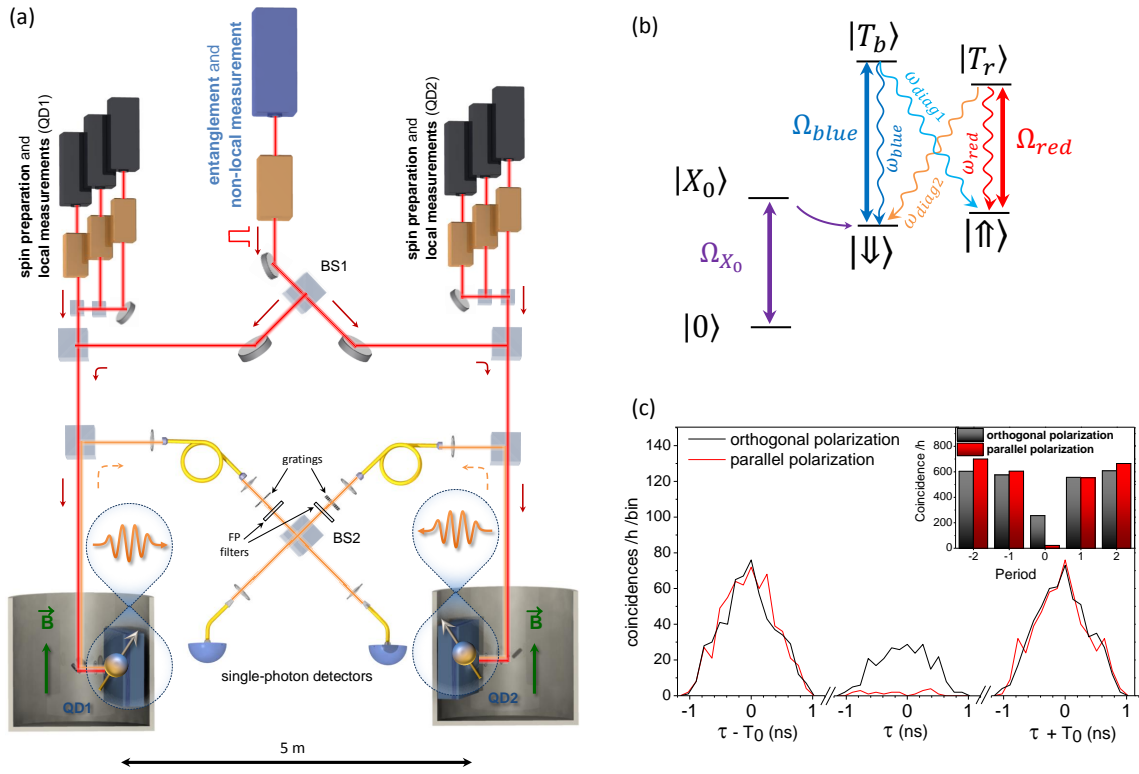


Figure 1. Experimental set-up. (A) Two bath cryostats separated by 5 meters host quantum dot samples in Voigt geometry. The quantum dots can be addressed by diode lasers (in black) for local state preparation and readout, and by a Ti:Sapphire laser (in blue) for entanglement generation and non-local measurement. (B) Energy level diagram of a single quantum dot. Upon excitation of the neutral exciton ($|X_0\rangle$) state, the electron can tunnel out, leaving behind a single hole. Application of a finite magnetic field gives rise to spin-dependent optical selection rules with four allowed transitions of identical oscillator strength. (C) Characterization of the indistinguishability of the Raman photons from the two dots with a Hong-Ou-Mandel experiment: coincidence counts on the two output arms of BS2 are plotted as a function of the delay between the recorded photon arrival times under pulsed excitation. T_0 is the repetition period of 52 ns. When the input modes have parallel polarizations (red curve), the coincidence counts within the time window (-1 ns, 1 ns) are 11 times smaller than for the case of the input modes having orthogonal polarization.

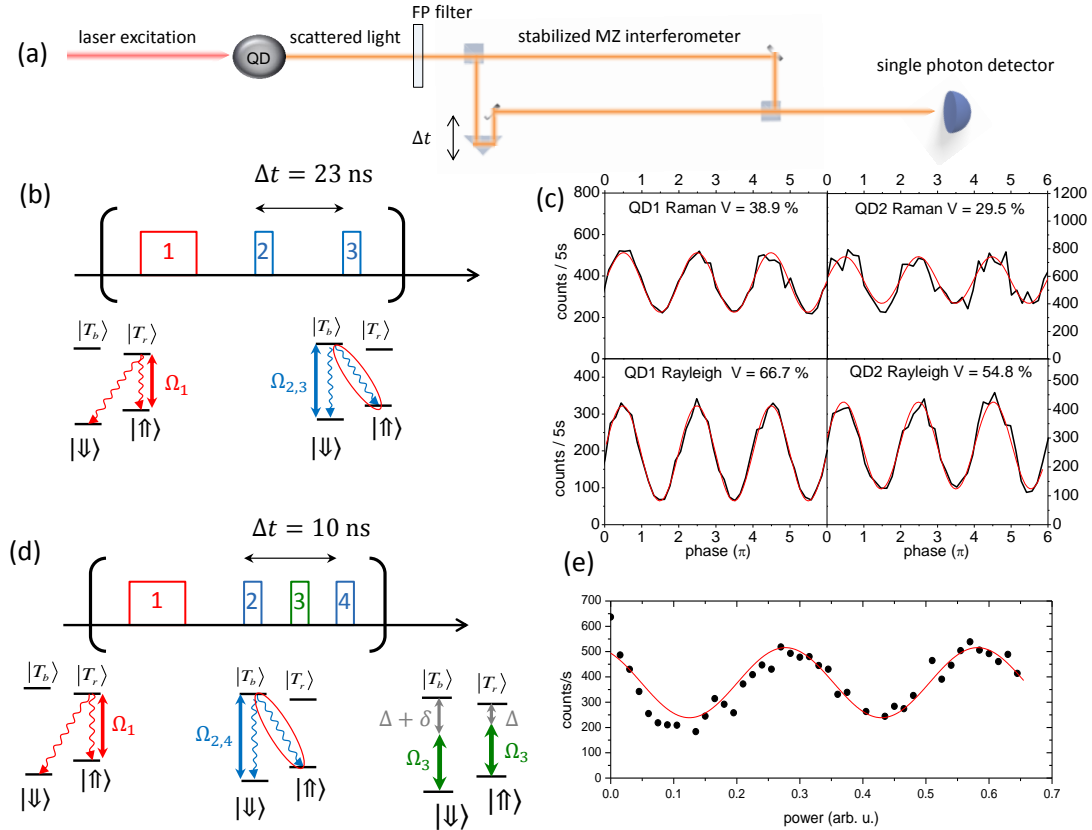


Figure 2. Coherence and rotation of the hole pseudo-spin. (A) Sketch of the experimental set-up for the single-photon interference of Raman scattered photons. The single photons are sent to an interferometrically stabilized Mach-Zehnder (MZ) interferometer of path length difference $c\Delta t$. A single photon detector is placed in one of the output modes of the second beam-splitter. (B) Pulse sequence used for the first order coherence measurement, and the relevant energy level diagram. We first apply a pulse of frequency ω_{red} to spin pump into the $|\downarrow\rangle$ state (pulse 1). We then apply two successive weak pulses (2 and 3) at frequency ω_{blue} . The time offset of the two pulses approximately matches the path length difference of the MZ interferometer. (C) Count rate of the single photon detector, for QD1 (left column) and QD2 (right column), when filtering only the Raman (upper row) or the Rayleigh (lower row) scattered photons, as a function of the phase difference in the two arms. The associated visibility, obtained from a sinusoidal fit of the count rate, is indicated in the associated panel. (D) Pulse sequence used to demonstrate pseudo-spin rotation about the z axis of the Bloch sphere: the pulse sequence is identical to the one used for part (B), with an additional detuned laser pulse of 4 ns (pulse 3) is inserted in between the two pulses at ω_{blue} (2 and 4). (E) Black dots: count rate of the output detector, as a function of the detuned laser power, demonstrating control of the pseudo-spin phase. Red curve: fit to the data.

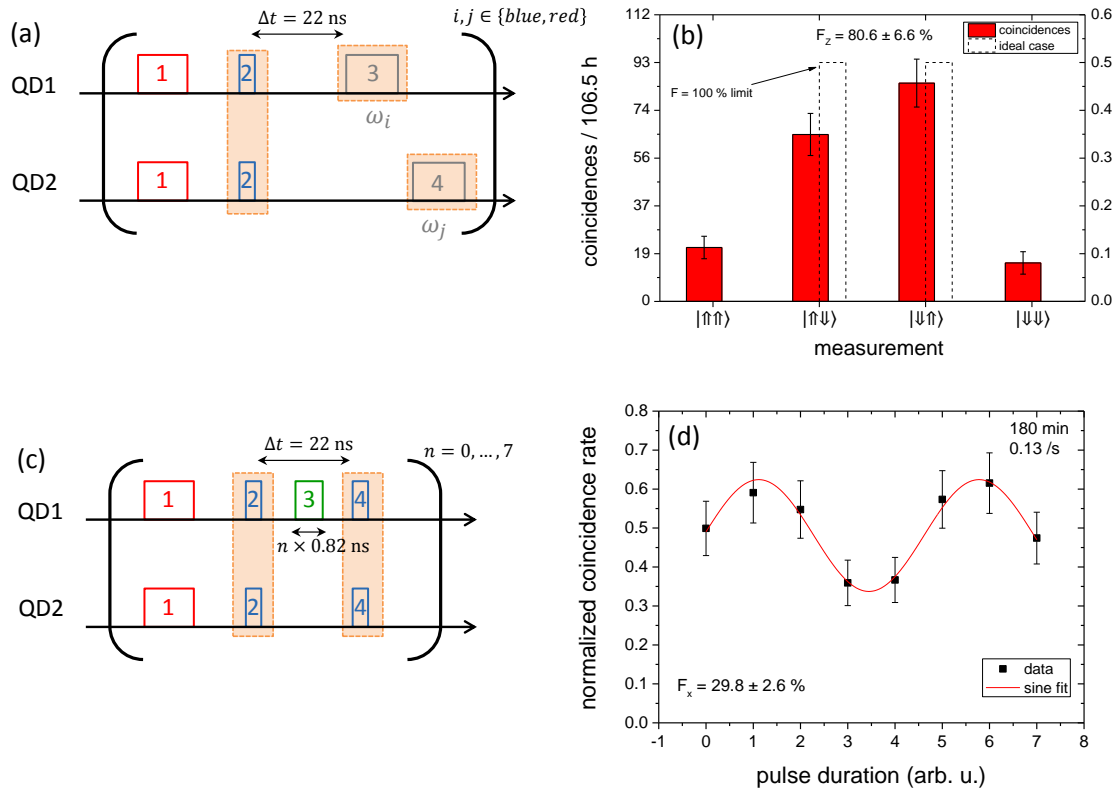


Figure 3. Characterization of the heralded entangled state. (A) Pulse sequence used for the measurement of classical correlations between the distant spins. After spin pumping into the $|\downarrow, \downarrow\rangle$ state (pulse 1), a weak entanglement pulse (pulse 2) is sent simultaneously to both quantum dots (QD1 and QD2). After 22 ns, pulse 3 measures the spin-state of QD1 and then pulse 4 measures the spin-state of QD2. The four measurement combinations are alternated. The total repetition period of the measurement processes is 4×104 ns. (B) Red bars: results of three-fold coincidences between a photon emitted during the entanglement pulse and a photon in each of the two measurement pulses (orange shading in Fig. 3a) obtained during a total measurement time span of 106.5 h. The dashed bars represents the ideal limit of vanishing even parity spin state detection. The error bars represent one standard deviation deduced from poissonian statistics of the raw detection events. The measured fidelity is $F_z = 80.6 \pm 6.6 \%$. (C) Pulse sequence used to measure quantum correlations between the distant spins. After spin pumping into the $|\downarrow, \downarrow\rangle$ state, a weak entanglement pulse (pulse 2) is used to drive both quantum dots. A detuned laser pulse (pulse 3) modifies the phase of the QD1 hole spin phase. After 22 ns, a non-local measurement pulse is applied to both QDs. The pulse sequence is repeated for different values of the duration of the pulse 3 ranging from 0 to 8×0.82 ns, corresponding to a laser-induced QD1 spin phase rotation ranging from 0 to 3π . (D) Black dots: two-fold coincidence rate between a photon detected during the entanglement pulse and a second photon detected during the measurement pulse (orange shading in Fig. 3c), normalized by the average detection rate between photons emitted during different periods, as a function of the pulse-length of pulse 3. The error bars represent one standard deviation deduced from poissonian statistics of the raw detection events. The red curve is a sinusoidal fit to the data, yielding a visibility of $V = 29.8 \pm 2.6 \%$.